

Pressure Induced Valence Transitions in f -Electron Systems

W. M. Temmerman,¹ A. Svane,² L. Petit,³ M. Lüders,¹ P. Strange,⁴ and Z. Szotek¹

¹*Daresbury Laboratory, Daresbury, Warrington WA4 4AD, UK*

²*Department of Physics and Astronomy, University of Aarhus, DK-8000 Aarhus C, Denmark*

³*Computer Science and Mathematics Division, and Center for Computational Sciences,
Oak Ridge National Laboratory, Oak Ridge, TN 37831, USA*

⁴*School of Physical Sciences, University of Kent, Canterbury, Kent, CT2 7NH, UK*

(Dated: May 7, 2019)

A review is given of pressure induced valence transitions in f -electron systems calculated with the self-interaction corrected local spin density (SIC-LSD) approximation. These calculations show that the SIC-LSD is able to describe valence changes as a function of pressure or chemical composition. An important finding is the dual character of the f -electrons as either localized or band-like. A finite temperature generalisation is presented and applied to the study of the p-T phase diagram of the $\alpha \rightarrow \gamma$ phase transition in Ce.

PACS numbers:

I. INTRODUCTION

The knowledge of valence of rare earth or actinide ions is important for the understanding of the solid state physical properties of f -electron systems. It determines for example the equilibrium volume of f -electron compounds. This is extremely well illustrated in work of Jayaraman^{1,2}. In Fig. 1 we show the lattice constants for the rare earth sulphides, selenides and tellurides (after Ref. 2). The abrupt expansion of the lattice for SmS, SmSe, SmTe, EuS, EuSe, EuTe, TmSe, TmTe, YbS, YbSe and YbTe is associated with a change in valence from trivalent rare earth to divalent rare earth. Hence this figure shows a direct correlation between lattice constants and valence. Whilst the determination of the valence is important for the static properties of f -electron systems, it becomes less useful for understanding the dynamical properties such as heavy fermion and Kondo screening of local spin magnetic moments. However it was shown³ that the construction of an alloy analogy for the valences can describe the finite temperature behaviour, in particular the pressure versus temperature phase diagram of Ce. Therefore dynamical fluctuations between valences could possibly describe the finite temperature behaviour of such systems as heavy fermions.

The f -electron systems are a rich hunting ground for structural and valence transitions as a function of pressure.^{4,5,6} Advances in experimental techniques, such as progress in high pressure cell technology, make pressure experiments feasible over an ever-increasing range, possibly up to 1000 kbar. Furthermore the constant improvements in brightness of the synchrotron sources allow for the study of high pressure phases of f -electron materials in greater detail.

In this paper we will review a methodology for ab initio calculations of valence and hence valence transitions as a function of pressure. The methodology is based on the self-interaction corrected local spin density (SIC-LSD) approximation. SIC-LSD corrects for a spurious self-interaction of an electron with itself. This self-

interaction is in most circumstances small and hence the LSD is sufficiently accurate for most applications. However for localized states this correction is substantial and the SIC-LSD approach needs to be applied. The SIC-LSD method differentiates between localized and itinerant electrons and leads to an orbital dependent potential. Hence, self-interaction corrections capture a dual picture of coexisting localized and band-like f -electrons.^{7,10} As a function of volume or pressure rearrangements in the number of localized and band-like f -electrons take place and a study of this forms one of the topics of this paper.

The paper is organized as follows. In Section II the basic aspects of the SIC-LSD method are outlined, concentrating on its implementation in terms of bands and k-points. In Section III we comment on the so-called local SIC implementation and its generalization to alloys and finite temperatures, allowing to study both static valence and spin fluctuations. Section IV contains the calculations of valence of elemental rare earths, their mono-sulphides and mono-nitrides. Also the results for the valences for Ce-, Sm-, Eu- and Yb-mono-pnictides and mono-sulphides are presented in that Section. Section V discusses the valences of the actinides and their compounds. The results for the $\alpha \rightarrow \gamma$ phase transition in Ce at finite temperatures is the subject of Section VI. Section VII presents the summary and conclusion.

II. THE SIC-LSD TOTAL ENERGY METHOD AND VALENCE

The total energy functional of the local spin density (LSD) approximation to density functional theory provides good accuracy in describing conventional solids with weakly correlated electrons.^{11,12} However, for all rare earths and for materials containing actinide elements (beyond Np) the electron correlations are significant, and the self-interaction correction needs to be included to obtain a similar accurate description of the localized nature of the $4f$ or $5f$ electrons.

The ensuing SIC-LSD total energy functional¹³ is derived from the LSD as:

$$E^{SIC-LSD} = E^{LSD} - \Delta E_{sic}, \quad (1)$$

$$E^{LSD} = T + U + E_{xc} + V_{ext} + E_{so}, \quad (2)$$

$$\Delta E_{sic} = \sum_{\alpha}^{occ.} \delta_{\alpha}^{SIC}, \quad (3)$$

$$E_{so} = \sum_{\alpha}^{occ.} \epsilon_{\alpha}^{so} \quad (4)$$

where α labels the occupied electron states and δ_{α}^{SIC} is the self-interaction correction for state α . As usual, E^{LSD} can be decomposed into a kinetic energy, T , a Hartree energy, U , the interaction energy with the atomic ions, V_{ext} , and the exchange and correlation energy, E_{xc} .¹⁴ Here in addition we include the spin-orbit coupling term E_{so} . The spin-orbit energy, for each occupied state α is:

$$\epsilon_{\alpha}^{so} = \langle \psi_{\alpha} | \xi(\vec{r}) \vec{l} \cdot \vec{s} | \psi_{\alpha} \rangle. \quad (5)$$

The ΔE_{sic} term expresses the spurious self-interaction of the LSD energy, which is subtracted from the LSD energy in equation (1). The self-interaction is calculated for each occupied state α , and is given by the sum of the Hartree interaction and the exchange-correlation energy for the charge density of that state:

$$\delta_{\alpha}^{SIC} = U[n_{\alpha}] + E_{xc}[n_{\alpha}]. \quad (6)$$

For itinerant states, δ_{α}^{SIC} vanishes identically, while for localized (atomic-like) states the self-interaction may be appreciable. Thus, the self-interaction correction constitutes a negative energy contribution gained by an f -electron when localizing, which competes with the band formation energy gained by the f -electron if allowed to delocalize and hybridize with the available conduction states. The volume dependence of δ_{α} is much weaker than the volume dependence of the band formation energy of rare earth $4f$ or actinide $5f$ electrons, hence the overbinding of the LSD approximation for narrow f band states is reduced when localization is allowed. The SIC-LSD energy functional in Eq. (1) appears to be a functional of all the one-electron orbitals, but can in fact be viewed as a functional of the total (spin) density alone, as discussed in Ref. 15.

One major advantage of the SIC-LSD energy functional is that it allows for different valence scenarios to be explored. By assuming atomic configurations with different total numbers of localized states, self-consistent minimization of the total energy leads to different local minima of the same functional, $E^{SIC-LSD}$ in Eq. (1), and hence their total energies may be compared. The configuration with the lowest energy defines the ground state configuration. Note, that if no localized states are assumed, $E^{SIC-LSD}$ coincides with the conventional LSD functional, i.e., the Kohn-Sham minimum of the E^{LSD} functional is also a local minimum of $E^{SIC-LSD}$. Among

the actinide elements, this was also found to be the global minimum for U and Np, but for the later actinide elements, and also in all rare earths, minima exist with a finite number of localized states.¹⁰ The reason is that the respective f orbitals are sufficiently confined in space to benefit appreciably from the self-interaction correction.

Another advantage of the SIC-LSD scheme is the possibility to localize f -states of different character. In particular the various crystal field eigenstates, either magnetic or paramagnetic.

The SIC-LSD still considers the electronic structure of the solid to be built from individual one-electron states, but offers an alternative description to the Bloch picture, namely in terms of periodic arrays of localized atom-centered states (*i.e.*, the Heitler-London picture in terms of Wannier orbitals). Nevertheless, there still exist states which will never benefit from the SIC. These states retain their itinerant character of the Bloch form, and move in the effective LSD potential. This is the case for the non- f conduction electron states in the rare earth and actinide metals.

Results of two implementations of the SIC-LSD scheme will be presented in this paper. The first approach applies the SIC to the localized bands, whilst in the second approach the SIC is applied to the phase shifts of the localized states. Both approaches can be considered to be a reasonable ansatz, for the solid state, to the implementation of the SIC for atoms. The latter approach is local in nature - as expressed by the use of single site phase shifts- whilst the former can take into account a more extended behaviour of the wave function. However the band-based approach involves repeated back and forth transformations of the wavefunctions from reciprocal space to real space localised functions. In real space the band-dependent SIC potential is evaluated, in reciprocal space the bandstructure problem is solved. This is a time consuming aspect of this method. Further details of this implementation can be found in Ref. 18. For a variety of applications to d and f electron solids, see Refs. 7,18,19,20,21 and references therein. The results in Sections IV and V are based on applying the SIC to the localized bands, whilst the finite temperature discussion of Section VI is based on the single site phase shifts and the so-called L(ocal)-SIC implementation³ in terms of multiple scattering theory, briefly outlined in the following section.

III. LOCAL SELF-INTERACTION APPROACH

In this local formulation of SIC we use the multiple scattering formalism and concentrate our attention on the phase shifts of electrons scattering from ions in a solid. If a phase shift is resonant it is reminiscent of a bound state at positive energies, i.e., above the zero of the potential which in this case is the muffin-tin zero. The energy derivative of the phase shift is related to the Wigner delay-time. If this is large the electron will

spend a long time on the site. Such 'slow' electrons will be much more affected by the spurious self-interaction and therefore should see an SI-corrected potential. Thus when the phase shift has a resonance we calculate the self-interaction correction in this (l, m) angular momentum channel. This is accomplished by calculating the one-electron charge density for this channel, which defines the charge density for the self-interaction correction potential to be added to the LSD potential. Then the phase shifts using the total (SIC-LSD) potential are recalculated. This is applied m channel by m channel for a particular angular momentum l . Like in the case of band by band SIC implementation, the minimization of the total energy determines the optimum configuration of (l, m) channels for self-interaction correction. Therefore we can associate with each of the m channels two potential functions, $V_{\text{eff}}^{\text{SIC-LSD}}(r)$ and $V_{\text{eff}}^{\text{LSD}}(r)$. If the total energies of these scenarios are sufficiently close, one can envisage dynamical effects playing an important role as a consequence of tunneling between these states.

Due to the multiple scattering aspect of this approach we can easily calculate Green's functions and from them various observables for making contact with experiments. Another advantage is that it can be easily generalized to include the coherent potential approximation,^{22,23,24,25,26} extending the range of applications to random alloys. In addition, one can use it to treat static correlations beyond LSD by studying pseudoalloys whose constituents are composed of e.g. two different states of a given system: one delocalized, described by the LSD potential, and another localized, corresponding to the SIC-LSD potential. Combined with the disordered local moments (DLM) formalism for spin-fluctuations,^{27,28} this allows also for different orientations of the local moments of the constituents involved. In addition, in this formulation we can generalize the SIC approach to finite temperature, T , to study its effect on the electronic total energies, E_{tot} , and the electronic contribution to the entropy.

To fully take into account the finite temperature effects, we calculate the free energy of a (pseudo)alloy, as a function of temperature, volume, V , and concentration, c , namely

$$F(T, c, V) = E_{\text{tot}}(T, c, V) - T \left(S_{\text{el}}(T, c, V) + S_{\text{mix}}(c) + S_{\text{mag}}(c) + S_{\text{vib}}(c) \right). \quad (7)$$

Here S_{el} is the electronic (particle-hole) entropy, S_{mix} the mixing entropy of the pseudoalloy, S_{mag} the magnetic entropy, and S_{vib} the entropy originating from the lattice vibrations.

The full extent of the L-SIC approach is illustrated in Section VI where we discuss the famous Ce $\alpha \rightarrow \gamma$ phase transition.

IV. LOCALIZATION/DELOCALIZATION AND VALENCE TRANSITIONS IN RARE EARTH COMPOUNDS

A. Valencies of rare earths, rare earth nitrides and rare earth sulphides

The change of the rare earth valence as a function of atomic number is one of the outstanding physical properties of elemental rare earths. Among the materials that exhibit valence changes are the rare earth elements and their sulphides where changes from trivalent to divalent are observed in SmS, Eu, EuS, Yb and YbS, whilst no valence transition is observed in the rare earth nitrides. The lattice constants of all pnictides, with the exception of Ce, behave continuously. In the sulphides (Fig. 1) changes of the lattice constants as large as 10% occur in the middle and at the end of the series. These are associated with a change in valence from trivalent to divalent in the sulphides whilst the pnictides remain trivalent. The discontinuous behaviour of the CeN lattice constant is due to tetravalency. The calculated SIC-LSD energy differences between divalent and trivalent configurations are presented in Fig. 2. One sees that at the beginning of the series the rare earths, their nitrides and sulphides are very solidly trivalent. This tendency for trivalency decreases towards the middle of the rare earth series where the curve more or less repeats itself from Gd onwards. The nitrides remain trivalent throughout the rare earth series whereas SmS, Eu, EuS, Yb and YbS become divalent. From Fig. 2 it is clear that the rare earth nitrides are most trivalent and the rare earth sulphides are least trivalent. The elemental rare earths are intermediate between the nitrides and sulphides. Whilst the trends are well reproduced, there is an overall tendency to overemphasize divalency. Thus all the results in Fig. 2 have been calibrated by 43 mRy to agree with the observed valence transition pressure of 6 kbar in SmS.²

Having firmly demonstrated that the behaviour of the lattice constants seen in Fig. 1 is caused by the valence behaviour, we can endeavour to ask why. In Fig. 3 the number of f -band electrons in the trivalent states is plotted. The crossover from the trivalent to divalent state occurs when the number of f -band electrons is above 0.7. At this point the localization energy wins over the band formation energy and it becomes more advantageous to localize an extra f electron. For the nitrides the number of occupied itinerant f -electron states stays well below 0.7 due to the strong hybridization with the nitrogen p -states. The nitrides remain trivalent throughout the rare earth series. With respect to this the application of the SIC-LSD is different between atoms and solids. In the case of atoms the levels are occupied in steps of one electron and the self-interaction is always applied. In the solid state the occupancy of a state can vary between zero and one and whether or not to apply the self-interaction is determined by a competition between the band formation energy (no self-interaction) and the lo-

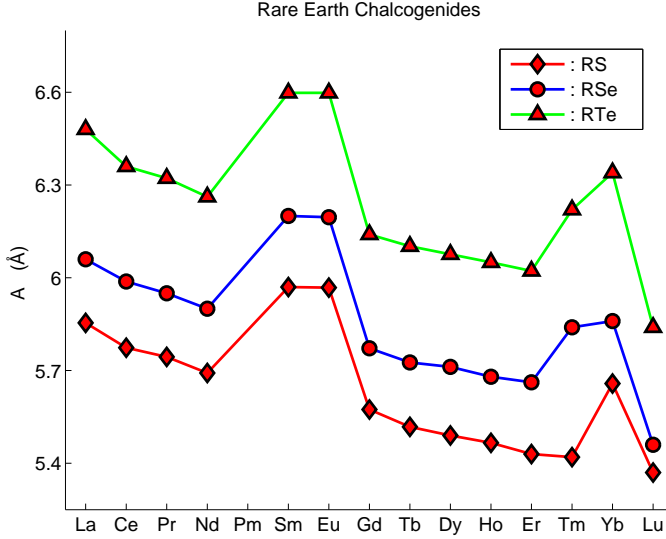


FIG. 1: Lattice constants of rare earth sulphides (after Jayaraman in Reference 2).

calization (application of the self interaction) of each of the bands. This leads to a definition of valence since the self interaction corrected localized states are well separated from the valence states and no longer available for bonding and band formation. In the following we will discuss some further applications for the mono-pnictides and mono-sulphides of Ce, Sm, Eu and Yb.

B. Ce monopnictides and monochalcogenides

Cerium and cerium compounds attract considerable attention due to the intricate electronic properties related to the Ce f -electrons. A variety of phenomena like heavy-fermion,^{29,30} mixed-valence³¹ and Kondo behaviour^{32,33} is encountered. The cerium monopnictides and monochalcogenides have peculiar properties as a function of applied hydrostatic pressure (see Table I).

With the SIC-LSD approach¹⁹, we have studied the high pressure behaviour of CeP, CeAs, CeSb, CeBi^{34,35}, CeS, CeSe and CeTe³⁶. For all these compounds we have found the trivalent Ce state to be the groundstate. The experimental lattice constants are reproduced within 1% accuracy. The results regarding pressure transitions are summarized in Table I, which contains all theoretically computed phase transition pressures and relative volumes on the low and high pressure sides of the transition (given as a fraction of the equilibrium volume at $P = 0$).

The total energy as a function of volume for CeP is calculated for each of the phases B1 and B2 and with the f -electron treated as either delocalized (normal band picture, as implemented with LSD) or localized (SIC-LSD). The results are shown in Fig. 4. The lowest energy is found in the B1 phase with localized f -electrons and with

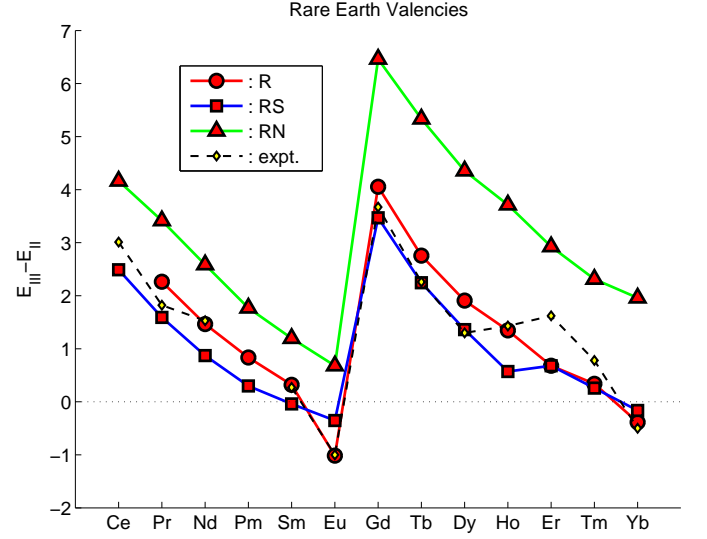


FIG. 2: Energy differences (in eV) between the divalent and trivalent configurations for the rare earths, their sulphides and nitrides.^{7,8} The dashed line shows the 'experimental' values for the rare earth metals.⁹ The circles, squares and triangles show the calculated values for the rare earth metals, the rare earth sulphides and the rare earth nitrides, respectively. The open circles and the crosses show the calculated values for the rare earth metals and the rare earth sulphides, respectively.

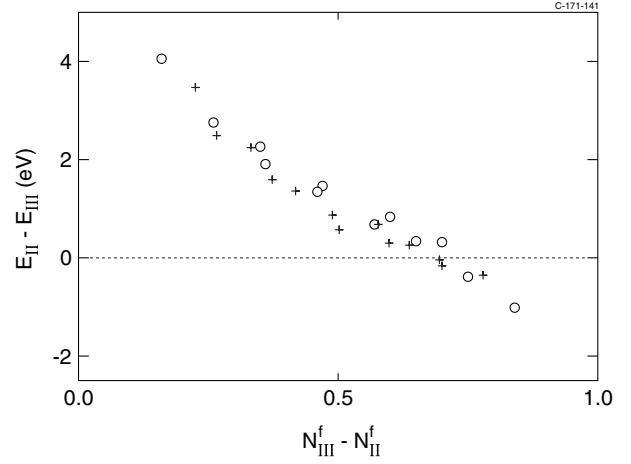


FIG. 3: The correlation between rare earth valence and the number of band-like f -electrons. Positive values on the y-axis mean trivalency. Negative values on the y-axis mean divalency. Note that for more than 0.7 f -band electrons the divalent configuration becomes more favourable.

a specific volume of 348 a_0^3 per formula unit, which coincides with the experimental equilibrium volume. The B1 phase with delocalized f -electrons has its minimum at a considerably lower volume, due to the significant f -electron band formation energy providing a large negative component to the pressure. From the common tangent a phase transition is predicted at a pressure of 71

kbar with a volume collapse of $\Delta V/V_0 = 8\%$ (change in volume relative to the zero pressure equilibrium volume), which is in excellent agreement with the transition seen at 55 kbar.³⁷ The B2 structure is not as favorable for the CeP compound, since the calculated energy is substantially higher than that of the B1 structure. This holds for both localized and delocalized f -electrons. From Fig. 4 we conclude that the B2 structure with localized f -electrons is never reached in CeP, while at high pressure a second phase transition to the B2 structure with delocalized f -electrons is found. The transition pressure is calculated to be 113 kbar and the volume collapse 12%, while experimentally the B1→B2 phase transition is seen at 150 ± 40 kbar.³⁸ The experimental volume collapse is 11 %. Some uncertainty is associated with comparing the total energies calculated for the B1 and B2 phases in the present approach. Therefore we have also investigated the high pressure transition in CeP with the full-potential LMTO method,³⁹ where no problem of this sort occurs. In this case we have found a transition pressure of 167 kbar, which is somewhat higher, but in good agreement with the experimental value.

The results reported in Table I show that all of the observed pressure transitions in the cerium pnictides and chalcogenides are indeed reproduced.^{34,35,36} The total energy curves look rather similar to those of CeP in Fig. 4, but minor changes in the relative positions occur when the ligand is varied. The localized phases are generally more favored when the ligand ion becomes heavier, and as a consequence, in CeAs no isostructural delocalization transition occurs in the B1 structure. Instead a transition directly from the B1 structure with localized f -electrons to the B2 structure with delocalized f -electrons occurs, in agreement with experiment. In CeSb and CeBi the first high pressure transition to occur is from B1 to B2, with localized f -electrons in both cases, and only at higher pressures is a delocalization transition predicted to take place. The calculated transition pressures are only slightly above the ranges studied experimentally. In this work only the B2 structure was considered for the second transition, but in reality the valence transition which eventually must take place in CeSb and CeBi may involve another high pressure phase.

In CeS the first transition occurs to the B1 phase with delocalized f -electrons, *i.e.*, the theory predicts an isostructural phase transition in CeS. The calculated transition pressure is 101 kbar with a volume collapse of 6%. These findings are in excellent agreement with the experiment of Ref. 40, but at variance with the results of Ref. 41, where no discontinuity in the pV -curve is observed. These results may indicate the proximity of a critical point. At higher pressures CeS transforms into the B2 phase. According to the present calculations this occurs in two steps. First, at a pressure of 243 kbar, CeS goes into the trivalent B2 phase with a 4.6% volume change. In the second step, at a pressure of 295 kbar, the tetravalent B2 phase is reached with a 3.6% volume collapse. Thus, CeS reenters the localized regime for a

very narrow pressure range. Some caution is necessary before accepting this rather peculiar behaviour. First of all the present calculations have been performed at $T = 0$ K, and thermal fluctuations might easily merge the two high-pressure transitions into one. Secondly, the SIC-LSD calculational scheme only implements rather idealized pictures of either completely localized or completely delocalized Ce f -electrons. Most likely, the Ce f -electrons enter into a complicated Kondo screened state in the B2 phase, which would alter the energetics of the B2 phase in a way we are currently not able to address. One could speculate that the Kondo screening at $T = 0$ K would interpolate between the ideal localized situation at large volumes and the ideal delocalized situation at small volumes. Depending on the details of this screening it could turn the transition into a continuous valence transition. Unfortunately, no experiments have been performed beyond 250 kbar.⁴² The almost certain theoretical prediction made here is that at high pressures the B2 phase will be reached. However, experimental verification is needed. Since we have found³⁴ that our present calculational approach tends to underestimate transition pressures for transitions from the B1 structure to the B2 structure, the experimental transition pressure for the B1→B2 transition in CeS would most likely be in the range of 300-350 kbar, which is easily within experimental reach. Of course, we can not rule out that other crystal structures may become important at high pressures. In elemental cerium as well as other rare earths, low-symmetry crystal phases occur when the f -electron delocalization sets in.^{7,43}

In both CeSe and CeTe the only pressure transition observed is that from B1 to B2 with localized f -electrons in both phases. These are also first to occur according to the calculations, while valence transitions are predicted in the range of 400 kbar. Thus, the situation here is quite similar to that in CeSb and CeBi, apart from the tetragonal distortion in these compounds which was not found for CeSe and CeTe.³⁶

C. Sm monpnictides and monochalcogenides

One of the most studied rare earth compounds is SmS^{50,51,52,53}. At low temperature and zero pressure it crystallizes in the NaCl structure exhibiting a semiconducting behaviour. At a moderate pressure of ~ 6.5 kbar SmS reverts to a metallic phase with a significant volume collapse of 13.5%⁵⁴, retaining however the NaCl structure. Valence transitions can also be brought about by alloying the SmS lattice with other trivalent ions, such as Y, La, Ce or Gd.^{50,55} Similar valence instabilities are observed in SmSe and SmTe^{51,56,57,58}, which also crystallize in the NaCl structure. For these compounds the volume changes continuously, but anomalously, with pressure (at room temperature)^{58,59}. From the photoemission studies it is concluded that SmSe and SmTe at ambient pressure, like SmS, are also of predominantly divalent f^6

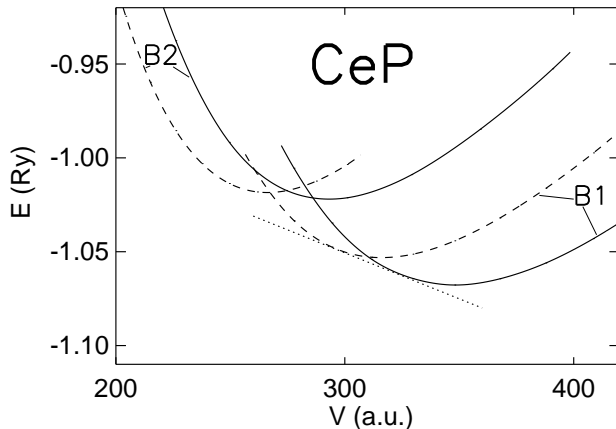
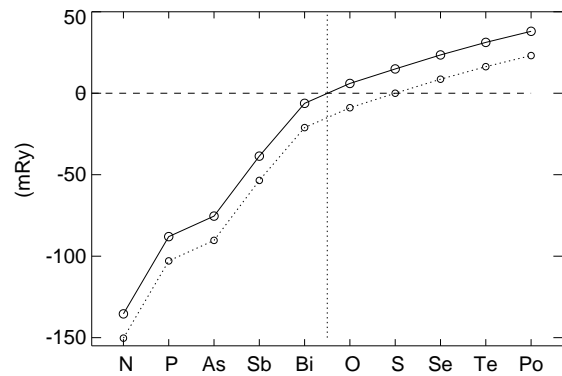


FIG. 4: Cohesive energy of CeP (in Ry/formula unit) as a function of specific volume (in a_0^3 /formula unit). Two crystal structures, the B1 and the B2, are considered, and each with two different treatments of the Ce f -electrons. The full drawn curves correspond to calculations with one localized f -electron per Ce atom, while the dashed curves correspond to itinerant f -electrons. The dotted line marks the common tangent at the isostructural phase transition in the B1 structure.

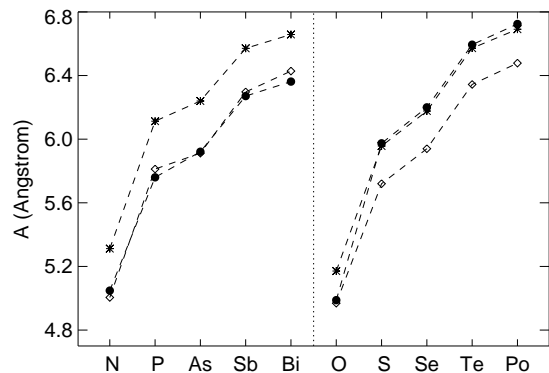
character⁵⁶ while the monpnictides show clear signals of pure trivalent f^5 ions^{56,60}.

Figure 5 shows the calculated lattice constants and valence stabilities for the Sm pnictides and chalcogenides^{61,62}. Specifically, the total energy difference is calculated for the scenarios of trivalent and divalent rare earth ions. A positive energy difference implies that the divalent configuration is preferred. For the Sm pnictides, the calculations reveal a strong preference for the f^5 configuration in the early pnictides, with the energy difference of 1.8 eV per formula unit in SmN. For the heavier Sm pnictides, the f^6 configuration becomes more and more advantageous, and for Bi it is only 0.08 eV higher than the trivalent configuration. This is the same trend towards more localised phases, as seen in the Ce compounds of the previous section, when the ligand ion becomes heavier.

Moving to the Sm chalcogenides, already in the Sm monoxide the f^6 configuration is found to be most favorable, by 0.08 eV, and in SmS by 0.20 eV. Hence, the SIC-LSD total energy predicts a valence transition of Sm between the Sm pnictides and the Sm chalcogenides. This is not in complete agreement with the experimental picture, according to which the divalent and intermediate-valent states are almost degenerate in SmS, while SmO is trivalent and metallic^{63,64}. Thus, it appears that the SIC-LSD total energy functional overestimates the tendency to form the divalent configuration of Sm, by approximately 15 mRy, in SmS. Assuming a similar error for all Sm compounds, this would imply that the calcu-



a)



b)

FIG. 5: a): Trivalent-divalent energy difference, $\Delta E = E(f^5) - E(f^6)$, of samarium compounds. Positive ΔE means divalent, negative ΔE means trivalent. The dashed line marks the calibrated curve⁶¹. b): Comparison of experimental and theoretical lattice constants of Sm mono-pnictides and monochalcogenides compounds.⁶¹ Experimental values are marked with solid circles, while lattice constants calculated assuming a divalent (trivalent) Sm ion are marked with stars (diamonds).

lated energy balance curve in Fig. 5 should be lowered by approximately 15 mRy. The dashed line of the figure shows the energy difference with such a correction. This switches the balance in favor of trivalency for SmO, in accord with experiments^{63,64}. Note that this is a reduction, due to the inclusion of the spin-orbit interaction, on the 43 mRy calibration energy quoted earlier and applied in Fig. 2. In other words, the spin-orbit interaction accounts for 28 mRy of the 43 mRy calibration energy. The remaining 15 mRy is therefore f - f correlations not accounted for by the SIC-LSD. The lattice constants are seen to be in excellent agreement with experimental value for all compounds, corroborating the conclusion that a valence shift occurs between SmO and SmS.

The trivalent phase of the chalcogenides becomes relevant at high pressure. In this phase the localised f^5 Sm ions coexist with a partly occupied narrow f -band, effectively describing an intermediate valent phase⁶¹. The

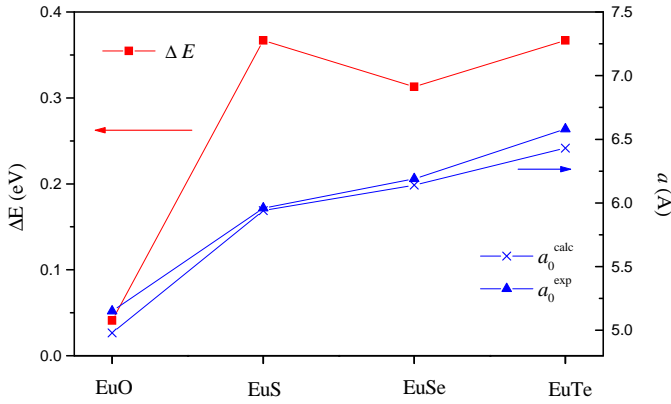


FIG. 6: The values of the lattice constant for the europium chalcogenides from experiment⁷¹ (triangles) and calculation⁶⁷ (crosses). Also shown is the calculated energy difference between the divalent and trivalent form (squares). The positive values mean divalent europium chalcogenides.

calculated and measured transition pressures are listed in Table II. The good agreement both for transition pressures and volume collapses proves that the bonding of the high pressure phase is well described in the SIC-LSD approximation, even if the true many-body wavefunction of the intermediate valence phase is much more complicated than the corresponding SIC-LSD wavefunction. This is in line with the general philosophy of the density functional approach of obtaining good total energy estimates from simple reference systems (non-interacting electrons). The present theory cannot describe the continuous nature of the transition observed for SmSe and SmTe. The experiments were all conducted at room temperature and it would be interesting to investigate whether the continuous transition would exist at low temperature as well.

D. Eu monpnictides and monochalcogenides

Europium chalcogenides and most of the pnictides crystallise in the simple NaCl crystal structure and hence form a series that can be studied within first principles theory relatively easily. Recently the chalcogenides have attracted a lot of attention due to their potential applications in spintronic and spin filtering devices.⁶⁶

The SIC-LSD method is applied to study the electronic structure of the Eu compounds in the assumed ferromagnetic state in both the divalent and trivalent configurations. Fig. 6 shows the calculated and experimental lattice constants for all the chalcogenides.⁶⁷ Also shown are the energy differences between the two valence states. It is clear that all the europium chalcogenides are divalent.

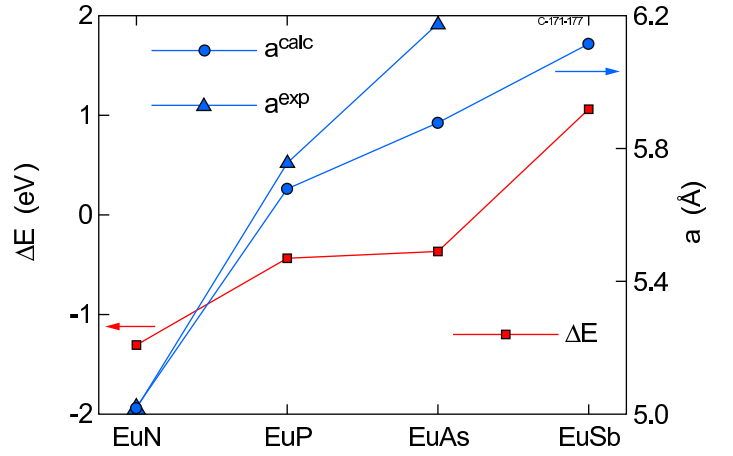


FIG. 7: The values of the lattice constant for the europium pnictides from the SIC-LSD calculation. The circles represent the calculated values⁶⁷ and the triangles are the experimental values.⁷³ Also shown is the calculated energy difference between the divalent and trivalent form. Negative values mean trivalent, positive values mean divalent.

This is as expected from simple shell-filling grounds. It can also be seen from this figure that the calculated lattice constants are in good agreement with experiment. The energy difference between the two valence states is fairly independent of chalcogenide for S, Se and Te and one can observe that there is a clear correlation between the lattice constant and the difference in energy between the divalent and trivalent states.

The calculated transition pressures for EuO and EuS are compared with experiment in Table III. The lower transition pressure and smaller volume in EuS compared to EuO is reproduced by the theory. Experimentally, the transition of EuO (at room temperature) is continuous, which the present theory cannot describe. For EuS the experiments show no anomalous compression curve⁶⁸, but the band gap closes at 160 kbar, just before the structural transition to the CsCl structure (at 200 kbar)⁷⁰. However due to the LMTO-ASA approximations, significant uncertainty persists in the values of the total energy differences between different crystal structures. Also the spin-orbit interaction can significantly alter the results: we found that without spin-orbit the structural transition occurs at 137 kbar¹⁹, however without an isostructural transition occurring first.

Fig. 7 shows the equilibrium lattice constants for the europium pnictides. Also shown are the energy differences between the divalent and trivalent configurations. It is clear that EuN, EuP and EuAs are trivalent and EuSb is divalent. These results are in full agreement with Hulliger⁷² who states that Eu ions in the EuN and EuP are known to be trivalent, while EuAs is known to contain some divalent ions. We are not aware of any definitive measurement of the valence state of EuSb, but clearly if the trend continues it will be divalent. Although the

calculation predicts that EuAs, with the rocksalt crystal structure, is trivalent, EuAs has in reality the Na₂O₂ crystal structure. This is a distortion of the NiAs structure due to the formation of anion-anion pairs.⁷² We speculate that the occurrence of Na₂O₂ crystal structure and divalent ions is intimately connected. These divalent ions do not occur in the rocksalt crystal structure and hence explain the theoretical underestimate in the value of the lattice constants as seen in Fig. 7. The presence of divalent ions in EuAs would also make the valence energy difference curve of Fig. 7 more continuous. These results are qualitatively similar to those obtained for the ytterbium pnictides^{74,75} (see below) where there is also an increasing tendency for divalency as we go down the pnictide column of the Periodic Table. However, in that case the divalent state is not reached.

E. Yb monpnictides and monochalcogenides

Here the application of the SIC-LSD method to Yb and a number of its compounds is discussed.^{74,75} We concentrate in particular on the valence of Yb ion in these systems, and some of the valence transitions, in particular in YbS. Fig. 8 shows for Yb compounds the f electron difference between the divalent and trivalent configurations versus their energy difference. The behaviour is close to linear. The closest we come to change of one electron occurs in YbN, specifically a change of 0.8 electrons, for which also the highest energy difference between the two electronic configurations is obtained. This maximum electron difference of 0.8 gradually decreases to approximately 0.5 for YbPd, YbSb, YbBi and YbBiPt and for the four divalent Yb systems we obtain between 0.22 to 0.35 electrons. For these divalent systems the difference in f electron count has nearly disappeared and this seems to herald the arrival of the divalent behaviour.

Our calculations can also make contact with the pressure-volume measurements which e.g. for YbS indicate anomalous behaviour around 100 kbar which could be associated with intermediate valence⁷⁶. In particular, for this system a trivalent state cannot seemingly be realized. In this case, our study could shed some light on properties of this intermediate valence state. From the common tangent construction of the total energies as a function of volume for both divalent and trivalent YbS, we obtain with the SIC approach a transition pressure which is ~ 75 kbar and agrees well with the experimental value of about ~ 100 kbar (Fig. 9). As seen in Fig. 9, the experimental anomaly is not really correlated with an integer change in valence, but is as a matter of fact due to an f electron delocalization. The quantitative theoretical description of this seemingly continuous valence transition calls for a more elaborate theory than presented here. The small change in f electron occupancy of 0.3 electrons found with the SIC approach upon delocalization of an f electron suggests the occurrence of intermediate valence of 2.3. This is consistent with the experimental estimate

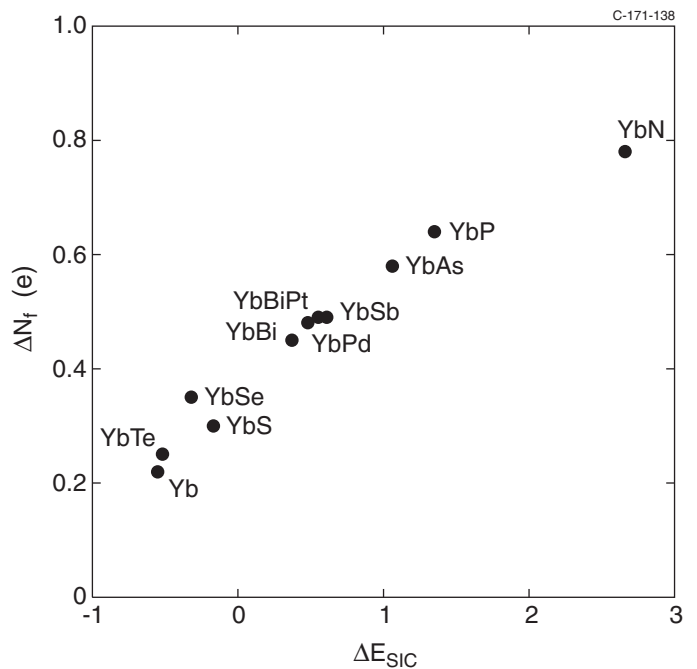


FIG. 8: Divalent-trivalent energy difference (in eV) of Yb compounds versus the total f -occupancy difference in the divalent and trivalent configurations, as given by the SIC-LSD approach.

of an intermediate valence of 2.4.⁷⁶

V. VALENCE TRANSITIONS IN ACTINIDE COMPOUNDS

A. Elemental actinides

Compared to the rare earth $4f$ -states, the $5f$ -states in the actinides are less inert, and in Th, Pa, and U, play an active role in the cohesion, as manifested by the low symmetry crystal structures, low specific volumes, and large bulk moduli. A localization transition occurs when going from Pu to Am,⁷⁷ and in the later actinides, from Am to Es, the f -electrons are non-bonding, high-symmetry crystal structures are attained, the specific volumes are large and the bulk moduli relatively small. Pu is situated at the borderline between these two competing pictures, and its very complex phase diagram implies that the f -electron properties are of particularly intricate nature. The low-symmetry α -Pu ground state is well reproduced by LDA calculations,⁷⁸ whilst the large-volume fcc phase of δ -Pu, is believed to be characterized by localized f -electrons.

The SIC-LSD approach was applied to the calculation of the total energies as a function of atomic volumes for the actinide elements from U to Fm.^{10,79} Ferromagnetic and paramagnetic arrangements were considered in the fcc structure, while antiferromagnetism was investigated

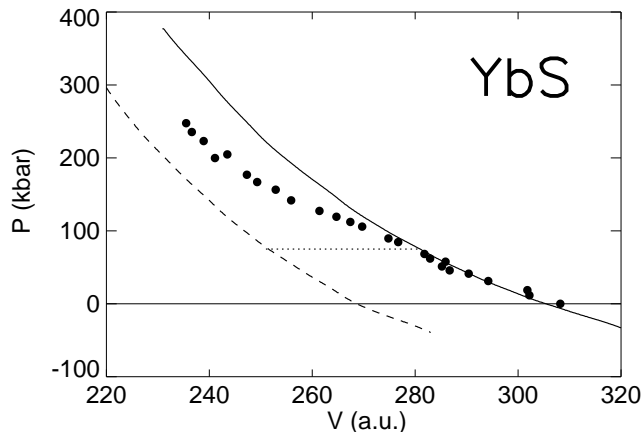


FIG. 9: Equation of state for YbS as calculated by the SIC-LSD method. The two theoretical curves correspond to 14 (solid line) and 13 (dashed line) localized f electrons, respectively, while the dots are the experimental data of Ref. 76. The dotted line marks the theoretical transition.

in the hcp structure. The overall total energy minima were found to occur for the trivalent configuration in the case of Am to Cf, while Es and Fm have their minima for the divalent state. Experimentally, Es is believed to be divalent, due to its large lattice constant, while Fm has never been prepared in the solid state. The U and Np metals have the lowest energies when the f -electrons are fully delocalized. The position of Pu at the crossover between localized and delocalized f -electron behaviour is revealed in the very different outcome of the calculations depending on the magnetism. In a magnetic calculation, the trivalent configuration has the lowest energy, however with a volume $\sim 30\%$ higher than the experimental volume of δ -Pu, while a paramagnetic treatment leads to virtual degeneracy of any of the localization scenarios f^0 to f^4 . The trends of the energy difference between the divalent and trivalent configurations are qualitatively the same in the actinides and the lanthanides and are governed by the relative stability of the half-filled f^7 shell. In Table IV, the calculated equilibrium volumes, bulk moduli, and transition pressures for onset of delocalization are shown. Overall, the experimental data are well reproduced by the SIC-LSD calculations.

The peculiar role played by Pu in the series of elemental actinides is illustrated in figure 10, which shows the total energy as a function of volume for all localization scenarios from f^0 to f^6 in a paramagnetic treatment. Remarkably, within 0.03 eV/atom the scenarios with 0,1,2,3 or 4 localized f -electrons are degenerate, while localizing 5 or 6 f -electrons is less favourable. The interpretation of this is that Pu at zero pressure exists in a complex quantum state vividly fluctuating between localized and delocalized f -electrons. This is in accord with the experimental observation of several allotropic forms of Pu,

including the low-volume α -phase and the high-volume δ -phase, the latter being only stable at elevated temperature or by alloying. In Table IV we compare the data of the f^4 state to the δ phase. If magnetic order is imposed, in either ferro- or antiferro-magnetic arrangement, the f^5 configuration becomes the ground state, i.e. formation of an ordered magnetic moment favours localization. The too large a volume associated with this solution indicates that this localization tendency is in fact overestimated, as the SIC-LSD formalism does not account properly for the strong quantum fluctuations taking place for a Pu ion in the metallic phase. Experimentally, there is no sign of magnetic moments in elemental Pu.⁸³

In Fig. 11 the total energy as a function of volume is shown for several f^n configurations in Am. As already mentioned, the trivalent f^6 configuration has the lowest energy, with an equilibrium volume of 201 a.u., while the experimental volume is 198 a.u.. Upon compression the band formation energy increases and the energy difference between f^5 and f^6 decreases. At a volume of about 140 a.u. the f^5 and f^6 total energy curves cross, and from then on the f -electron band states start to dominate. Around $V = 100$ a.u. the f -delocalization is complete. This is in good agreement with the experimental observation of a structural phase transition (AmII-AmIII) taking place at 100 kbar and at a compression corresponding to 77% of the equilibrium volume,⁸⁴ which is interpreted as the onset of f -bonding in Am. A rough theoretical estimate of the transition pressure, given by the slope of the $E(V)$ curves at the crossing point, leads to a value of 160 kbar. This estimate constitutes an upper bound to the delocalization pressure, since the high-valence SIC-LSD configurations represent a rather limited many-body wavefunction for a correlated state with actively bonding f -electrons. In addition, the correct (orthorhombic) high pressure phase was approximated here by the fcc structure, and finite temperature may also lower the phase transition pressure. Experimentally, the occurrence of the AmIV phase at $V/V_0 = 0.63$ at $p = 175$ kbar probably marks the endpoint of the f -electron delocalization process in Am.

Figure 12 shows the upper bounds for a transition pressure to a phase with bonding f -electrons. The agreement with experiment varies across the series, but is generally not bad (within a factor of 2). This qualitative agreement shows that the magnitude of the SIC-LSD localization energy is roughly correct. Figure 12 also shows the comparison of the volume ranges over which f -electron delocalization occurs for the actinide elements Pu, Am, Cm and Bk, as given by this theory and experiment. The qualitative trend as given by the relative stability of Cm(f^7), is well reproduced by the calculations, with a tendency of the calculated end-points of f -transition to be at too low a volume.

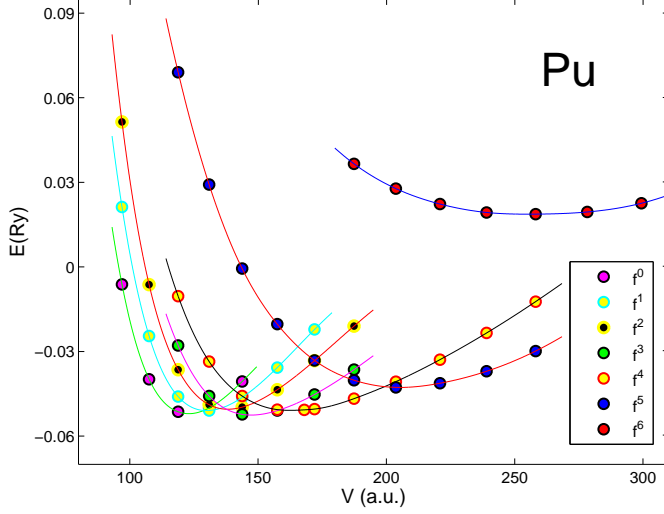


FIG. 10: Total energy of Pu in the paramagnetic fcc state.

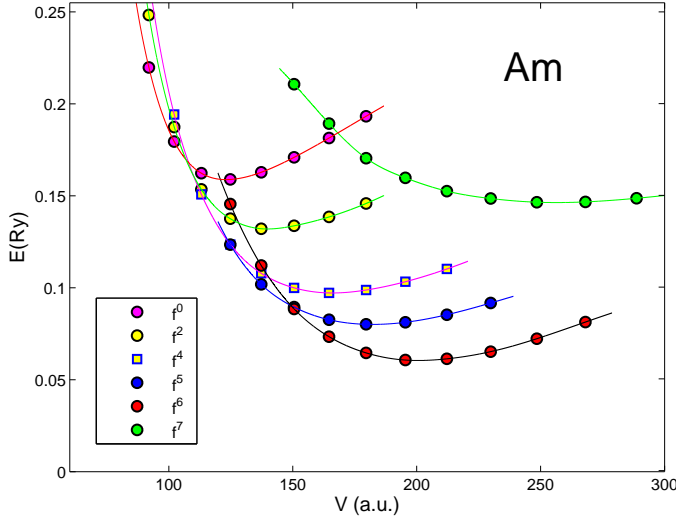


FIG. 11: Total energy versus volume for Americium in the paramagnetic fcc structure. Several configurations of the localized $5f$ subshell are considered.

B. Actinide monpnictides and monochalcogenides

In the actinide monpnictides and monochalcogenides, which all crystallize in the NaCl structure at ambient conditions, the actinide-actinide separations are larger than in the elemental metals, and the tendency towards f -electron localization can already be observed from Np compounds onwards. Figure 13 displays the calculated SIC-LSD ground state configurations through the series of U-, Np-, Pu-, Am-, and Cm-mono-pnictides and -mono-chalcogenides. The calculations reveal clear trends towards more and more actively bonding f -electrons for

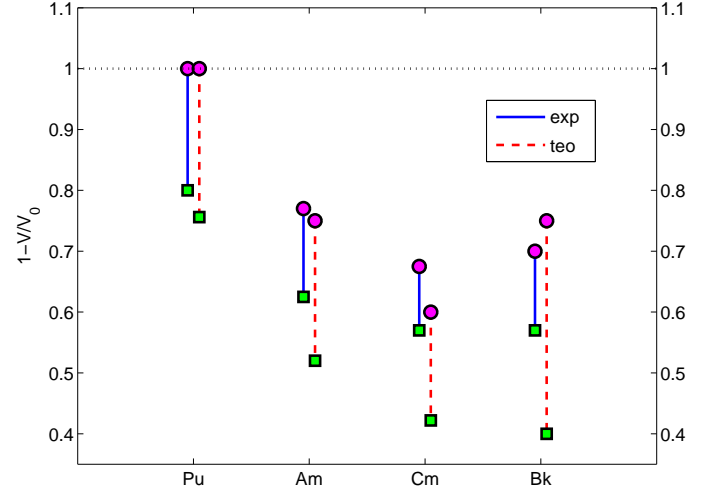


FIG. 12: Trends in the ranges of volumes of f electron delocalization in the actinide elements. Onset (completion) of delocalization is marked with balls (squares), for each element with experimental data (blue and full line) to the left and theoretical data (red and dashed line) to the right. Volumes are given relative to the (localized) equilibrium volume at ambient conditions. Experimental ranges are defined by the smallest volumes observed in the high-symmetry (fcc) phase and the largest volumes observed for the low-symmetry (α -U type) phases in high pressure experiments (Refs. 82,84,85; for Pu the range is defined by the zero pressure volumes of the δ - and α -phases). The theoretical ranges are calculated within the fcc structure only.

a) lighter actinides, and b) lighter ligands. For the lighter actinides, the f -orbitals are more extended, leading to larger overlaps with their nearest neighbours, and smaller self-interaction corrections, both of these effects favouring band formation. For the lighter ligands, in particular N and O, both the volume is decreased and ionicity is larger, the first of these effects leading to larger direct actinide-actinide overlap, and the latter effect favouring charge transfer.

The Cm compounds are the most localized systems, all exhibiting Cm in the trivalent f^7 configuration. The f^7 shell is so stable that variations of the ligand cannot disrupt its stability, and scenarios with either one more or less localized f -electron have distinctly higher energies. Trivalency prevails in the Am-compounds, but the stability of the f^7 shell causes the divalent Am state to be important in AmTe and AmPo. In the Pu compounds, the trivalent state also dominates, but for the lighter ligands f -electron delocalization sets in. In the Np compounds the tetravalent state dominates, while in the U compounds pentavalent states occur for the lighter ligands.

The density of states (DOS) of the actinide arsenides are shown in Fig. 14, with both trivalent and tetravalent actinide ions. In the trivalent case, the non-(SIC) f -degrees of freedom give rise to narrow unoccupied bands

N	O	<u>AcX valencies</u>									
P	S										
As	Se										
Sb	Te										
Bi	Po										
		U	Np	Pu	Am	Cm					
		65 5	5 54	5 54	3 3	3 3					
		5 54	4 4	4 3	3 3	3 3					
		4 54	4 4	3 3	3 3	3 3					
		4 4	4 4	3 3	3 3	3 3					
		4 4	3 3	3 3	3 2	3 3					

FIG. 13: Trends in localization through the AcX series. For each actinide, Ac=U, Np, Pu, Am, Cm, a block of 10 ligands are considered; the pnictides X=N, P, As, Sb, Bi, and the chalcogenides X= O, S, Se, Te, and Po. The numbers designate the calculated Ac valence for that particular AcX compound. Where two numbers are given, the corresponding valences are degenerate.

above the Fermi level. In the tetravalent case the additional delocalized f -electron appears as an extra f -band. In Cm, this band appears far below the Fermi level, while in Am, Pu and Np this band lies just below the Fermi level. The band formation due to this extra band is sufficiently large in NpAs to outweigh the localization energy, and the tetravalent configuration becomes the ground state.

C. Uranium compounds UPt_3 and UPd_3

Using the SIC-LSD method, we have similarly studied the 5 f valence configurations of U in UPt_3 and UPd_3 .⁸⁶ Both compounds are isoelectronic as far as the valence electrons are concerned, however the 5 d electrons are less tightly bound to the nucleus than the 4 d electrons, which results in a increased overlap of the U f and the transition metal d orbitals in UPt_3 . Correspondingly, the total energy calculations determine the tetravalent f^2 and the pentavalent f^1 configurations for UPd_3 (Fig. 15a) and UPt_3 (Fig. 15d) respectively. The calculated equilibrium volumes, $V_{\text{UPd}_3} = 474.1(\text{a.u.}^3)$ and $V_{\text{UPt}_3} = 469.7(\text{a.u.}^3)$, compare well with the experimental values of $V_{\text{UPd}_3}^{\text{exp}} = 469.5(\text{a.u.}^3)$ and $V_{\text{UPt}_3}^{\text{exp}} = 472.9(\text{a.u.}^3)$.⁸⁹ In both UPd_3 and UPt_3 , the small energy differences between the tetravalent and pentavalent configurations indicate near degeneracy (within ~ 5 mRy), rather than a clearly preferred f^2 groundstate for UPd_3 and an f^1 groundstate for UPt_3 . This in a way mirrors the results from XPS measurements, where in UPt_3 a weak shoulder at the Fermi energy indicates the presence of itinerant

5 f electrons,⁸⁷ and in UPd_3 this same shoulder is seen about 1 eV below the Fermi level, and is interpreted in terms of localized f electrons.⁸⁸ Sharp features, usually associated with localized f -electrons, are not observed. In $\text{UPt}_{3-x}\text{Pd}_x$ alloys, gradually substituting Pt by Pd, leads to a transition from the pentavalent to tetravalent groundstate between UPt_2Pd and UPtPd_2 , as can be seen from Figs. 15c and 15b respectively. An additional f -electron gets localized, a transition that appears to be driven mainly by the changes in the electronic structure related to the decreasing fd hybridization when replacing Pt by Pd. The opposite effect is obtained by putting UPd_3 under pressure. The total energy calculations for UPd_3 show that the pentavalent configuration becomes energetically favourable at pressures of approximately 250 kbar. From the observed similarities in the pentavalent DOS of both UPd_3 and UPt_3 ,⁸⁶ and given that UPt_3 is a heavy fermion material at zero pressure, we expect UPd_3 to become heavy fermion under pressure. Experimental efforts⁹⁰ to see the proposed transtion of UPd_3 under pressure failed. This can be either due to an underestimate in the present theory of the transition pressure, or finite temperature effects in the experiment.

VI. VALENCE TRANSITION IN CE AT FINITE TEMPERATURE

Cerium is the first element in the Periodic Table that contains an f electron, and shows an interesting phase diagram.⁹¹ In particular, the isostructural (fcc \rightarrow fcc) $\alpha - \gamma$ phase transition is associated with a 15%-17% volume collapse and total quenching of the magnetic moment.⁹¹ The low-pressure γ -phase shows a local magnetic moment, and is associated with a trivalent configuration of Ce ion. At the temperatures in which the γ -phase is accessible, it is in a paramagnetic disordered local moment state. Increasing the pressure, the material first transforms into the α -phase, which is indicated to be in an intermediate valence state with quenched magnetic moment. At high pressures (50 kbar at room temperature) Ce eventually transforms into the tetravalent α' -phase. With increasing temperature, the $\alpha - \gamma$ phase transition shifts to higher pressures, ending in a critical point (600K, 20 kbar), above which there is a continuous crossover between the two phases.

To describe the full phase diagram of the Ce $\alpha - \gamma$ phase transition we have modelled Ce as a pseudoalloy,^{92,93} in the spirit of the Hubbard III approximation⁹⁴, consisting of the trivalent (SIC-LSD) Ce atoms with concentration c , and the tetravalent (LDA) Ce atoms with the concentration (1- c). In order to properly take into account the disordered local moments of the trivalent Ce atoms in the γ -phase, equal probabilities for up and down orientations of their local moments were adopted. Assuming homogeneous randomness, this ternary pseudoalloy can be described by the coherent potential approximation (CPA). The respective concentrations of the trivalent and the

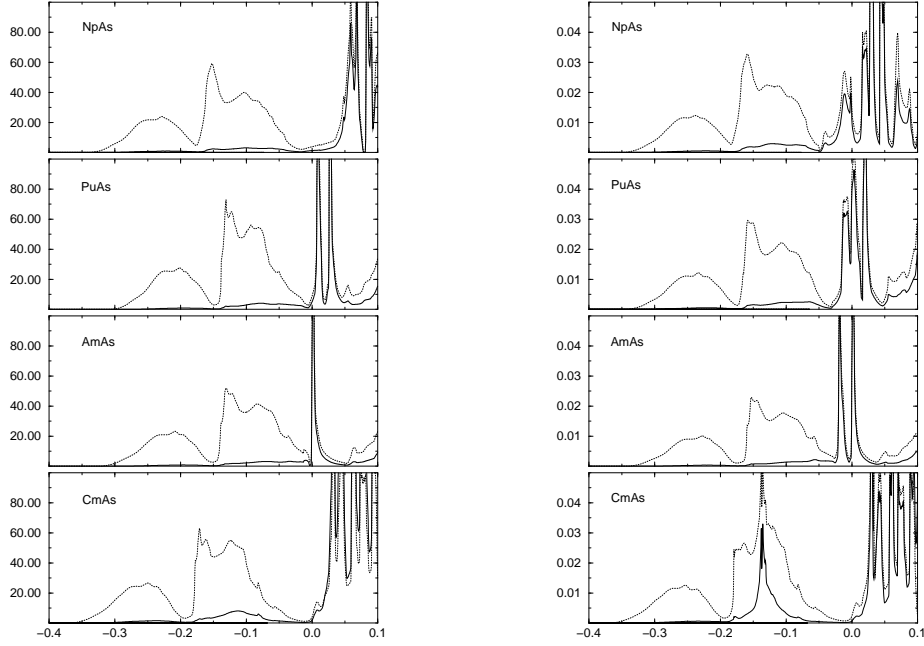


FIG. 14: Densities of states (in states/(Ry formula unit)) for the actinide arsenides NpAs, PuAs, AmAs, CmAs, with a trivalent (left), or tetravalent (right) actinide ion, respectively. The solid and dotted lines represent the f projected- and total densities of states, respectively. The energies are given in Ry, with the Fermi level at energy zero.

tetravalent Ce ions in the pseudoalloy are then determined by minimizing the free energy for each volume and temperature with respect to the concentration c .

The free energy of the physical system at a given volume can be obtained by evaluating the concentration dependent free energy at the minimizing concentration c_{\min} :

$$F(T, V) = F(T, c_{\min}, V). \quad (8)$$

These free energies are displayed in Fig. 16, which clearly shows a double-well behaviour, corresponding to the two separate phases of Ce, at low temperatures, which is gradually smoothed out with increasing temperatures. Furthermore one finds that, at elevated temperatures, the free energy is mainly lowered for large lattice constants, corresponding to the γ -phase, with its larger entropy. Inserting the minimizing concentration c_{\min} into the pressure-volume relation

$$p(T, V) = p(T, c_{\min}, V) = -\frac{\partial}{\partial V} F(T, c_{\min}, V), \quad (9)$$

allows to calculate the isotherms of Ce, which are displayed in Fig. 17. It can be seen that the average valence, close to the coexistence line, gradually changes with increasing temperature. Above the critical temperature, the valence changes continuously with increasing pressure from trivalent to tetravalent Ce ion.

In Fig. 18 we present the phase diagram, obtained from the free energies of the α - γ pseudoalloy, with the

γ -phase described by the DLM approach. It can clearly be seen in the figure how the transition becomes continuous above the critical temperature. The experimentally observed critical point (600K, 20 kbar) falls on top of the calculated phase separation line, which starts at the zero temperature transition pressure of -7.4 kbar. This means that the slope of the phase separation line is in very good agreement with experiments. The calculated critical temperature overestimates the experimental one by roughly a factor of 2, which is still reasonable considering that the critical temperature is very sensitive to various small details of the calculations and in particular the theoretical lattice parameters of both the Ce phases. Note that our calculated value of 169 K for the T_c at zero pressure compares well with the experimental value of 141 ± 10 K.

Finally we examine in more detail the discontinuity across the phase separation line. Fig. 19 shows the magnitude of the discontinuities for the various contributions of the Gibbs free energy. As expected, all contributions vanish at the critical temperature, above which there is a continuous cross-over between the α - and the γ -phase. It also can be seen from this figure that the entropy discontinuity is by far the largest contribution. The phase transition is therefore driven by entropy, rather than by energetics. The entropy discontinuity itself is mainly due to the magnetic entropy. Thus it is the entropy, and not the internal energy that drives the Ce α - γ phase transition. Analysis of experimental data leads to the same conclusion.⁹⁵

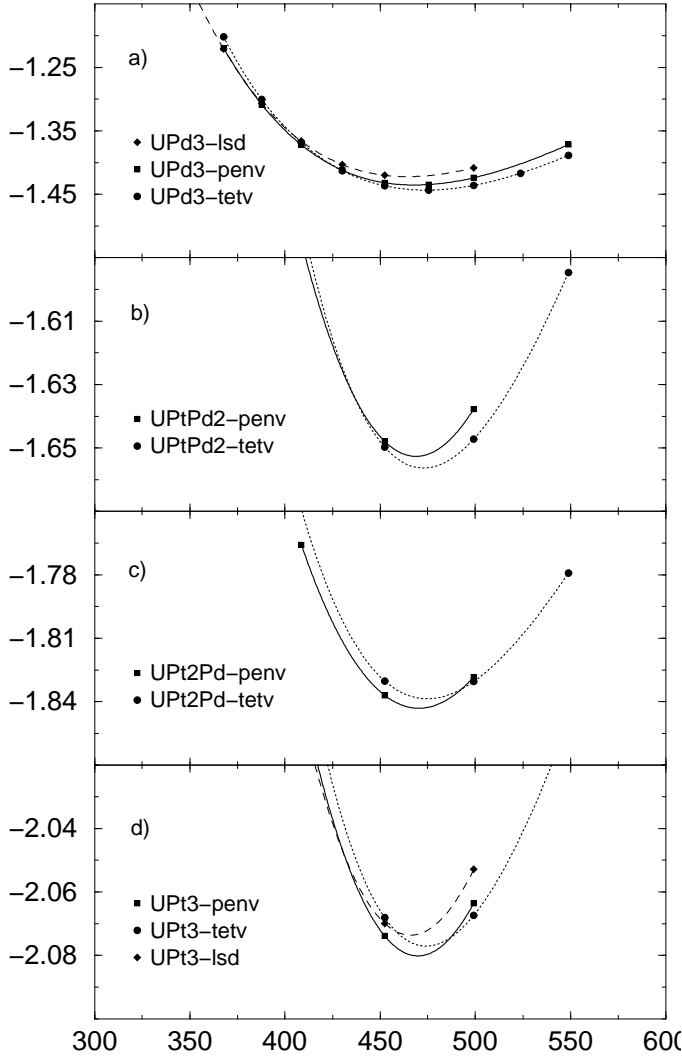


FIG. 15: Total Energy (in Ry/f.u.) versus volume (in (a.u.)³) for a) UPd₃, b) UPtPd₂, c) UPt₂Pd, and d) UPt₃.

VII. SUMMARY AND CONCLUSION

In this article a review has been given of some applications of the SIC-LSD to the calculation of the valences of f -electron systems. A methodology has been presented which is able to determine valence changes as a function of pressure and chemical composition. An important finding of this work is the discovery of the dual character of f electrons. The number of localized f -electrons defines the valence. Furthermore, a correlation between a change in valence and the number of band-like f -electrons has been established.

The versatility and functionality of the SIC-LSD has increased with the L-SIC. In particular as the example of the p-T plot in Fig. 18 shows a finite T generalization of the method has been successfully developed. This will

allow us to perform the finite T study of the p-V curves

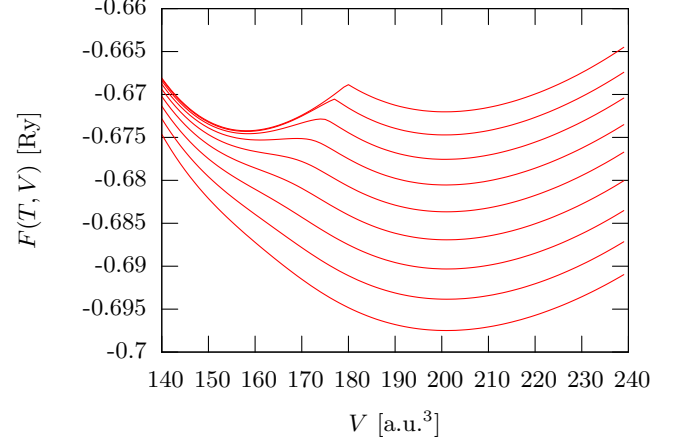


FIG. 16: The free energies as function of the volume for the temperatures 0 (highest curve), 200, 400, 600, 800, 1000, 1200, 1400 and 1600 K (lowest curve). The zero of energy is arbitrary.

of several of the compounds discussed in this paper and to determine if the continuous transitions as some times seen experimentally can be obtained.

VIII. ACKNOWLEDGEMENTS

This work was partially funded by the EU Research Training Network (contract:HPRN-CT-2002-00295) 'Ab-initio Computation of Electronic Properties of f -electron Materials'. AS acknowledge support from the Danish Center for Scientific Computing. Work of LP was sponsored by the Office of Basic Energy Sciences, U.S. Department of Energy.

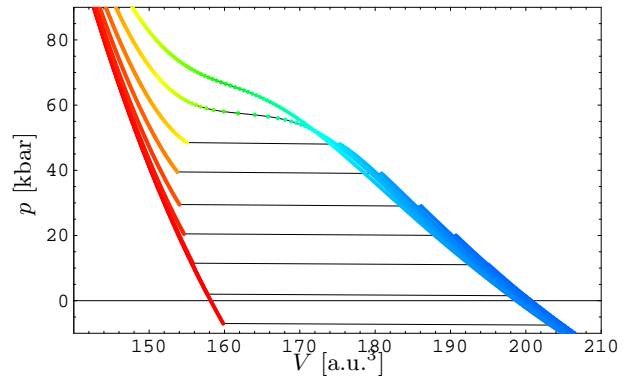


FIG. 17: Calculated isotherms for the temperatures $T=0$ (lowest curve), 200, 400, 600, 800, 1000, 1200, 1400, and, 1600K (highest curve). The color indicates the fraction of localized electrons: blue is all localized (γ -phase) and red is all delocalized (α -phase).

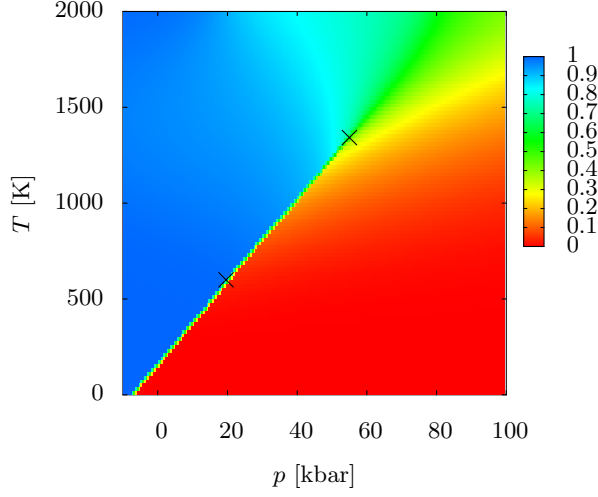


FIG. 18: Phase diagram obtained for the pseudoalloy, composed of α - and γ -Ce. The crosses indicate the calculated and experimental critical points.

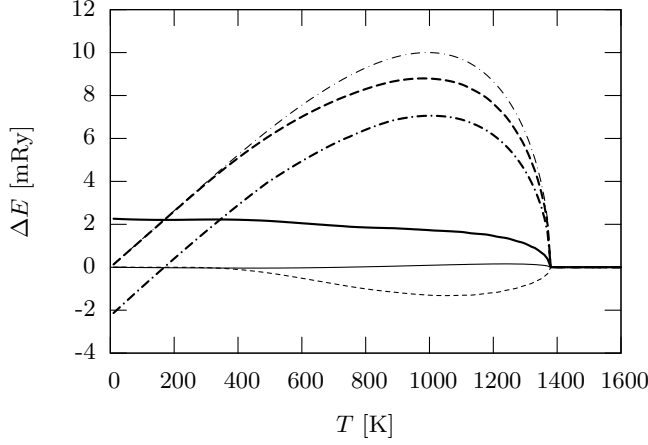


FIG. 19: Discontinuities of the total energy (thick solid line), the total entropy TS (thick dashed line) and the pV term (thick dashed-dotted line) over the phase separation line as function of the temperature. The entropy term is further decomposed into the electronic (thin solid line), the mixing (thin dashed line) and the magnetic (thin dashed-dotted line) contribution.

-
- ¹ A. Jayaraman in *Handbook on the Physics and Chemistry of Rare Earths; Volume1:Metals*, ed. by K.A. Gschneidner, Jr. and L. Eyring (North-Holland Publishing Company, 1978), p.707
- ² A. Jayaraman in *Handbook on the Physics and Chemistry of Rare Earths; Volume1:Alloys and Intermetallics*, ed. by K.A. Gschneidner, Jr. and L. Eyring (North-Holland Publishing Company, 1979), p.575
- ³ M. Lüders, A. Ernst, M. Däne, Z. Szotek, A. Svane, D. Ködderitzsch, W. Hergert, B. L. Györfy, and W. M. Tem-

- merman, Phys. Rev. B **71**, 205109 (2005)
- ⁴ Ichimin Shirotnani, Keigo Yamanashi, Junichi Hayashi, Yuu Tanaka, Naoki Ishimatsu, Osamu Shimomura and Takumi Kikegawa, J. Phys.: Condens. Matter **13** 1939 (2001).
- ⁵ Ichimin Shirotnani, Junichi Hayashi, Keigo Yamanashi, Kouji Hirano, Takafumi Adachi, Naoki Ishimatsu, Osamu Shimomura and Takumi Kikegawa, Physica B **334** 167 (2003).
- ⁶ N. V. Chandra Shekar and P. CH. Sahu, J Mater Sci **41** (2006)

- ⁷ P. Strange, A. Svane, W.M. Temmerman, Z. Szotek, and H. Winter, *Nature* **399**, 756 (1999).
- ⁸ C.M. Aerts, P. Strange, M. Horne, W.M. Temmerman, Z. Szotek, and A. Svane, *Phys. Rev. B* **69**, 045115 (2004).
- ⁹ B. Johansson, *Phys. Rev. B* **20**, 1315 (1979).
- ¹⁰ L. Petit, A. Svane, W. M. Temmerman, and Z. Szotek, *Solid State Commun.* **116**, 379 (2000).
- ¹¹ R. O. Jones and O. Gunnarsson, *Rev. Mod. Phys.* **61**, 689 (1989).
- ¹² R. M. Martin, *Electronic Structure*, (Cambridge University Press, 2004).
- ¹³ J. P. Perdew and A. Zunger, *Phys. Rev. B* **23**, 5048 (1981).
- ¹⁴ P. Hohenberg and W. Kohn, *Phys. Rev.* **136**, B864 (1964); W. Kohn and L. J. Sham, *Phys. Rev. A* **140**, 1133 (1965).
- ¹⁵ A. Svane, *Phys. Rev. B* **51**, 7924 (1995).
- ¹⁶ M. R. Pederson, R. A. Heaton, and C. C. Lin, *J. Chem. Phys.* **82**, 2688 (1985).
- ¹⁷ A. Svane, N. E. Christensen, L. Petit, Z. Szotek, and W. M. Temmerman, *Phys. Rev. B* (submitted 2006).
- ¹⁸ W. M. Temmerman, A. Svane, Z. Szotek and H. Winter, in *Electronic Density Functional Theory: Recent Progress and New Directions*, Eds. J. F. Dobson, G. Vignale and M. P. Das (Plenum, NY 1998.), p. 327.
- ¹⁹ A. Svane, P. Strange, W. M. Temmerman, Z. Szotek, H. Winter, and L. Petit, *phys. stat. sol. (b)* **223**, 105 (2001).
- ²⁰ L. Petit, A. Svane, Z. Szotek, P. Strange, H. Winter, and W. M. Temmerman, *J. Phys.: Condens. Matter* **13**, 8697 (2001).
- ²¹ L. Petit, A. Svane, Z. Szotek and W.M. Temmerman, *Science* **301**, 498 (2003).
- ²² P. Soven, *Phys. Rev.* **156**, 809 (1967).
- ²³ G. M. Stocks, W. M. Temmerman, B. L. Gyorffy, *Phys. Ref. Lett.* **41**, 339 (1978).
- ²⁴ B. L. Gyorffy and G. M. Stocks, in *Electrons in Disordered Metals and at Metallic Surfaces*, edited by P. Phariseau, B. L. Gyorffy, and L. Scheire, Plenum Press NATO'ASI Series Physics B42 (1979).
- ²⁵ J. S. Faulkner and G. M. Stocks, *Phys. Rev. B* **23**, R5628 (1981).
- ²⁶ G. M. Stocks and H. Winter, in *The Electronic Structure of Complex Systems*, edited by P. Phariseau and W. M. Temmerman, Plenum Press NATO'ASI Series Physics B113 (1984).
- ²⁷ B. L. Gyorffy, A. J. Pindor, J. B. Staunton, G. M. Stocks, and H. Winter, *J. Phys. F* **15**, 1337 (1985).
- ²⁸ J. B. Staunton, B. L. Gyorffy, G. M. Stocks, and H. Winter, *J. Phys. F* **16**, 1761 (1986).
- ²⁹ G.R. Stewart, *Rev. Mod. Phys.* **56**, 755 (1984).
- ³⁰ P. Fulde, J. Keller and G. Zwicknagl, in *Solid State Physics*, edited by H. Ehrenreich, D. Turnbull (Academic, New York, 1988), Vol. 41, p. 1
- ³¹ *Valence Fluctuations in Solids*, Edited by L. M. Falicov, W. Hanke, and M. B. Mable, (North-Holland, Amsterdam, 1981).
- ³² G. Aeppli and Z. Fisk, *Comments Condens. Matter. Phys.* **16**, 155 (1992).
- ³³ J. W. Allen and R. M. Martin, *Phys. Rev. Lett.* **49**, 1106 (1982); R. M. Martin and J. W. Allen, *J. Magn. Mat.* **47&48**, 257 (1985).
- ³⁴ A. Svane, Z. Szotek, W. M. Temmerman, and H. Winter, *Solid State Commun.* **102**, 473 (1997).
- ³⁵ A. Svane, Z. Szotek, W. M. Temmerman, J. Lægsgaard, and H. Winter, *J. Phys.:Condens. Matter*, **10**, 5309 (1998).
- ³⁶ A. Svane, W. M. Temmerman, and Z. Szotek, *Phys. Rev. B* **59**, 7888 (1999).
- ³⁷ N. Mori, Y. Okayama, H. Takahashi, Y. Haga and T. Suzuki, *Physica B* **186-188**, 444 (1993).
- ³⁸ I. Vedel, A. M. Redon, J. Rossat-Mignod, O. Vogt and J. M. Leger, *J. Phys. C* **20**, 3439, (1987).
- ³⁹ M. Methfessel, *Phys. Rev. B* **38**, 1537 (1988); M. Methfessel, C. O. Rodriguez, and O. K. Andersen, *Phys. Rev. B* **40**, 2009 (1989).
- ⁴⁰ M. Croft and A. Jayaraman, *Solid State Commun.* **35**, 203 (1980).
- ⁴¹ I. Vedel, A. M. Redon, J. M. Léger, J. Rossat-Mignod, and O. Vogt, *J. Phys. C* **19**, 6297 (1986).
- ⁴² J. M. Léger, *Physica B* **190**, 84 (1993).
- ⁴³ A. K. McMahan, C. Huscroft, R. T. Scalettar, and E. L. Pollock, *J. Computer-Aided Mater. Design*, **5**, 131 (1998).
- ⁴⁴ A. Werner, H. D. Hochheimer, R. L. Meng and E. Bucher, *Physics Lett.* **97A**, 207, (1983).
- ⁴⁵ J. M. Leger, D. Ravot and J. Rossat-Mignod, *J. Phys. C* **17**, 4935, (1984).
- ⁴⁶ J. M. Leger, K. Oki, J. Rossat-Mignod and O. Vogt, *J. de Physique* **46**, 889, (1985).
- ⁴⁷ J. M. Leger and A. M. Redon, *J. Less-Common Met.* **156**, 137 (1989).
- ⁴⁸ J. M. Léger, R. Epain, J. Loriers, D. Ravot, and J. Rossat-Mignod, *Phys. Rev. B* **28**, 7125 (1983).
- ⁴⁹ The experimental transition pressures are given as the middle of the hysteresis loop with error bars given by the extremes of the hysteresis loop. The quoted experimental volumes at the low- and high-pressure sides of the transition are the volumes as given by the experimental pV -curves at the middle of the hysteresis loop.
- ⁵⁰ P. Wachter, *Handbook on the Physics and Chemistry of Rare Earths*, Vol. 19, Chapter 132 (1994).
- ⁵¹ A. Jayaraman, V. Narayanamurthi, E. Bucher, and R. G. Maines, *Phys. Rev. Lett.* **25**, 1430 (1970).
- ⁵² C. M. Varma, *Rev. Mod. Phys.* **48**, 219 (1976).
- ⁵³ C. M. Varma and V. Heine, *Phys. Rev. B* **11**, 4763 (1975).
- ⁵⁴ U. Benedict and W. B. Holzapfel, in *Handbook on the Physics and Chemistry of Rare Earths*, Vol. 17, ed. by K. A. Gschneidner, L. Eyring, G. H. Lander, and G. R. Choppin, (North-Holland, Amsterdam 1993) Chapter 113.
- ⁵⁵ A. Jayaraman and R. G. Maines, *Phys. Rev. B* **19**, 4154 (1979).
- ⁵⁶ M. Campagna, E. Bucher, G. K. Wertheim and L. D. Longinotti, *Phys. Rev. Lett.* **33**, 165 (1974).
- ⁵⁷ V. A. Sidorov, N. N. Stepanov, L. G. Khvostantsev, O. B. Tsiok, A. V. Golubkov, V. S. Oskotski, and I. A. Smirnov, *Semicond. Sci. Technol.* **4**, 286 (1989).
- ⁵⁸ T. Le Bihan, S. Darracq, S. Heathman, U. Benedict, K. Mattenberger, O. Vogt, *J. Alloys. Comp.* **226**, 143 (1995).
- ⁵⁹ A. Chatterjee, A. K. Singh, and A. Jayaraman, *Phys. Rev. B* **6**, 2285 (1972).
- ⁶⁰ R. A. Pollak, F. Holtzberg, J. L. Freeouf, and D. E. Eastman, *Phys. Rev. Lett.* **33**, 820 (1974).
- ⁶¹ A. Svane, V. Kanchana, G. Vaitheeswaran, G. Santi, W. M. Temmerman, Z. Szotek, P. Strange and L. Petit, *Phys. Rev. B* **71**, 045119 (2005).
- ⁶² A. Svane, G. Santi, Z. Szotek, W. M. Temmerman, P. Strange, M. Horne, G. Vaitheeswaran, V. Kanchana, L. Petit and H. Winter, *phys. stat. sol. (b)* **241**, 3185 (2004).
- ⁶³ J. M. Leger, P. Aimonino, J. Loriers, P. Dordor, and B. Coqblin, *Phys. Lett.* **80A**, 325 (1980).
- ⁶⁴ G. Krill, M. F. Ravet, J. P. Kappler, L. Abadli, J. M.

- Leger, N. Yacoubi, and C. Lorigers, Solid State Commun. **33**, 351 (1980).
- ⁶⁵ O. B. Tsiok, V. A. Sidorov, V. V. Bredikhin, L. G. Khvostantsev, A. V. Golubkov, and I. A. Smirnov, Solid State Commun. **79**, 227 (1991).
- ⁶⁶ P. LeClair, J.K. Ha, H.J.M. Swagten, J.T. Kohlhepp, C.H. van de Vin, and W.J.M. de Jonge, Applied Physics Letters **80**, 625 (2002).
- ⁶⁷ M. Horne, P. Strange, W.M. Temmerman, Z. Szotek, A. Svane and H. Winter, J. Phys.: Condens. Matter **16**, 5061 (2004)
- ⁶⁸ A. Jayaraman, A. K. Singh, A. Chatterjee, and S. Usha Devi, Phys. Rev. B **9**, 2513 (1974).
- ⁶⁹ H. G. Zimmer, K. Takemura, K. Syassen, and K. Fischer, Phys. Rev. B **29**, 2350 (1984).
- ⁷⁰ K. Syassen, Physica B **139 & 140**, 277 (1986).
- ⁷¹ M. Gasgnier, *Handbook on the Physics and Chemistry of Rare Earths*, Vol. 5, chapter 41 (1984).
- ⁷² F. Hulliger, *Handbook on the Physics and Chemistry of Rare Earths*, Vol. 4, chapter 33, p218 (1984).
- ⁷³ P. Villars and L.D. Calvert, in *Pearson's Handbook of Crystallographic Data for Intermetallic Phases*, 2nd edn (Metals Park, OH: ASM International)
- ⁷⁴ W.M. Temmerman, Z. Szotek, A. Svane, P. Strange, H. Winter, A. Delin, B. Johansson, O. Eriksson, L. Fast and J.M. Wills, Phys. Rev. Lett. **83**, 3900, (1999).
- ⁷⁵ A. Svane, W.M. Temmerman, Z. Szotek, L. Petit, P. Strange and H. Winter, Phys. Rev. B. **62**, 13394, (2000).
- ⁷⁶ K. Syassen, H. Winzen, H.G. Zimmer, H. Tups, and J.M. Leger, Phys. Rev. B. **32**, 8246, 1985
- ⁷⁷ B. Johansson, and H. L. Skriver, J. Magn. Magn. Mat. **29**, 217 (1982)
- ⁷⁸ M. D. Jones, J. C. Boettger, R. C. Albers, and D. J. Singh, Phys. Rev. B **61**, 4644 (2000).
- ⁷⁹ A. Svane, L. Petit, Z. Szotek, and W. M. Temmerman, preprint (2006).
- ⁸⁰ J. Donohue, *The Structures of the Elements*, Wiley, New York (1974).
- ⁸¹ C.A. Calder, E.C. Draney, W.W. Wilcox, J. Nucl. Mater. **97**, 126 (1981)
- ⁸² U. Benedict, J. R. Peterson, R. G. Haire, and C. Dufour, J. Phys. F: Met. Phys. **14**, L43 (1984); R. G. Haire, J. R. Peterson, U. Benedict, and C. Dufour, J. Less-Comm. Met. **102**, 119 (1984).
- ⁸³ J. C. Lashley, A. Lawson, R. J. McQueeney, and G. H. Lander, Phys. Rev. B. **72**, 054416 (2005).
- ⁸⁴ S. Heathman, R. G. Haire, T. Le Bihan, A. Lindbaum, K. Litfin, Y. Meresse, and H. Libotte, Phys. Rev. Lett. **85**, 2961 (2000).
- ⁸⁵ S. Heathman, R. G. Haire, T. Le Bihan, A. Lindbaum, M. Idiri, P. Normile, S. Li, R. Ahuja, B. Johansson, and G. H. Lander, Science, **309**, 110 (2005).
- ⁸⁶ L. Petit, A. Svane, W.M. Temmerman, and Z. Szotek, Phys. Rev. Lett. **88**, 216403 (2002).
- ⁸⁷ W. D. Schneider and C. Laubschat, Phys. Rev. B **23**, 997 (1981).
- ⁸⁸ Y. Baer *et al.*, Solid State Commun. **36**, 387 (1980).
- ⁸⁹ P. Villars and L. D. Calvert, *Pearson's Handbook of Crystallographic Data for Intermetallic Phases*, 2. ed., (ASM International, Ohio, 1991).
- ⁹⁰ S. Heathman, M. Idiri, J. Rebizant, P. Boulet, P. S. Normile, L. Havela, V. Sechovsky and T. Le Bihan, Phys. Rev. B **67**, 180101(R) (2003)
- ⁹¹ D. C. Koskenmaki and K. A. G. Jr., in *Handbook on the physics and chemistry of rare earths*, edited by K. A. G. Jr. and L. Eyring, p. 337, North-Holland, Amsterdam, New York, Oxford, 1978.
- ⁹² B. Johansson, I. A. Abrikosov, M. Alden, A. V. Ruban and H. L. Skriver, Phys. Rev. Lett. **74**, 2335 (1995).
- ⁹³ A. Svane, Phys. Rev. B **53**, 4275 (1996).
- ⁹⁴ J. Hubbard, Proc. R. Soc. London **A 281**, 401 (1964).
- ⁹⁵ B. Amadon, S. Biermann, A. Georges, and F. Aryasetiawan, Phys. Rev. Lett. **96**, 066402 (2006).

TABLE I: Calculated transition pressures for the electronic and structural phase transitions in the cerium monopnictides and monochalcogenides. Also quoted are the specific volumes (relatively to the zero pressure equilibrium volume) on the two sides of the transition Ref. 49. The notation (d) and (l) refers to calculations with delocalized or localized Ce f -electrons, i.e. tetravalent or trivalent Ce atoms. B2* denotes the distorted B2 structure. The subscripts refer to the following references: a: Ref. 38; b: Ref. 37; c: Ref. 44; d: Ref. 45; e: Ref. 46; f: Ref. 42; g: Ref. 40; h: Ref. 47; i: Ref. 48; j: Ref. 5.

compound	transition	P_t (kbar)		V_1/V_0		V_2/V_0	
		theo.	expt.	theo.	expt.	theo.	expt.
CeN	B1(d) \rightarrow B2(d)	620	-	0.760	-	0.724	-
CeP	B1(l) \rightarrow B1(d)	71	$90^a, 55^b$	0.933	0.89^a	0.853	0.85^a
CeP	B1(d) \rightarrow B2(d)	113	$150(40)^a, 250^j$	0.827	0.82^a	0.706	0.71^a
CeAs	B1(l) \rightarrow B2(d)	114	$140(20)^c, 210^j$	0.893	0.84^c	0.713	0.73^c
CeSb	B1(l) \rightarrow B2*(l)	70	$85(25)^d, 150^j$	0.922	0.90^d	0.813	0.80^d
CeSb	B2*(l) \rightarrow B2*(d)	252	-	0.717	-	0.680	-
CeBi	B1(l) \rightarrow B2*(l)	88	$90(40)^e$	0.897	0.87^e	0.789	0.78^e
CeBi	B2*(l) \rightarrow B2*(d)	370	-	0.666	-	0.638	-
CeS	B1(l) \rightarrow B1(d)	101	$-^f, 125(15)^g$	0.918	0.93^g	0.855	0.88^g
CeS	B1(d) \rightarrow B2(l)	243	-	0.788	-	0.742	-
CeS	B2(l) \rightarrow B2(d)	295	-	0.724	-	0.688	-
CeSe	B1(l) \rightarrow B2(l)	124	$170(30)^h$	0.890	0.86^h	0.779	0.77^h
CeSe	B2(l) \rightarrow B2(d)	377	-	0.683	-	0.652	-
CeTe	B1(l) \rightarrow B2(l)	74	$55(25)^i$	0.915	0.93^i	0.798	0.84^i
CeTe	B2(l) \rightarrow B2(d)	435	-	0.647	-	0.623	-

TABLE II: Calculated isostructural transition pressures, P_t (in GPa; 1 GPa=10 kbar), and volume changes (in %), of Sm monochalcogenides. Experimentally, the transition of SmS is discontinuous, while those of SmSe and SmTe (at room temperature) are continuous.

The subscripts refer to the following references: d : Ref. 54; e : Insulator-metal transition of Ref. 57; f : Present author's estimates from figures of Ref. 58 and g : Ref. 65. The volume changes for SmSe and SmTe are obtained by extrapolation over the transition range.

Compound	P_t (GPa)		Volume collapse (%)	
	Theory	Expt.	Theory	Expt.
SmS	0.1	$0.65^d, 1.24^e$	11.1	$13.5^d, 13.8^e$
SmSe	3.3	$\sim 4^d, 3.4^e, 3 - 9^f, 2.6 - 4^g$	9.8	$8^d, 11^f, 7^g$
SmTe	6.2	$2 - 8^d, 5.2^e, 6 - 8^f, 4.6 - 7.5^g$	8.4	$9^f, 7^g$

TABLE III: Calculated isostructural transition pressures, P_t (in GPa; 1 GPa=10 kbar), and volume changes (in %), of Eu monochalcogenides.

The subscripts refer to the following references: a : Ref. 68; b : Ref. 69; c : Insulator-metal transition, Ref. 70

Compound	P_t (GPa)		Volume collapse (%)	
	Theory	Expt.	Theory	Expt.
EuO	19.3	$30^a, 13 - 30^b$	6.3	5^a
EuS	11.6	16^c	5.7	0^c

TABLE IV: Calculated^{10,79} and experimental equilibrium volumes, V , bulk modulii, B , and f -electron delocalization pressure, P , for the actinide elements. The magnetic ground state was used for Cm onwards, while the nonmagnetic was used for Pu and Am. Experimental values are from Ref. 82, except ^a: Ref. 80, and ^b: Ref. 81.

	V_{teo} (a.u.)	V_{exp} (a.u.)	B_{teo} (GPa)	B_{exp} (GPa)	P_{teo} (GPa)	P_{exp} (GPa)
α -Pu	123.0(-9%)	135 ^a				
δ -Pu	163.8(-2.5%)	168 ^a	46.0	32 ^b	0	~ 0
Am	200.6(+1.3%)	198	46.0	45	16	10
Cm	203.8(+0.9%)	202	42.4	33(5)	70	43
Bk	197.6(+6%)	189	35.0	25(5)	15	25
Cf	201.8(+9%)	185	37.3	49(5)	30	41
Es	256.0(-4.1%)	267, 321	19.5	-	11	-
Fm	247.4	-	29.6	-	28	-